Changes in wave climate and its impact on the coastal erosion in Samborombón Bay, Río de la Plata estuary, Argentina

Guido L. Bacino[a,b], Walter C. Dragani[a,c,d,*], Jorge O. Codignotto[a,b]

[a] CONICET, Consejo Nacional de Investigaciones Científicas y Técnicas, Godoy Cruz 2290, C1425FQB, Ciudad Autónoma de Buenos Aires, Argentina
[b] Servicio Geológico Minero Argentino (SEGEMAR), Av. General Paz 5445, B1650WAB, Provincia de Buenos Aires, Argentina
[c] Servicio de Hidrografía Naval, Av. Montes de Oca 2124, C1270ABV, Ciudad Autónoma de Buenos Aires, Argentina
[d] Instituto Franco-Argentino para El Estudio Del Clima y Sus Impactos (UMI FAECI/CNRS-CONICET-UBA), Ciudad Universitaria, Pabellón II, 2do. Piso, C1428EGA, Ciudad Autónoma de Buenos Aires, Argentina

1. Introduction

The loss of coastal wetlands, such as salt marshes, seems to be one of the consequences of the climatic change, because their locations within the intertidal zone make them vulnerable to erosive processes. Consequently, in the face of new environmental conditions, the coast is gradually adjusted to the long-term effects (Nicholls, 2011). In general, salt marshes are in a delicate balance between the lateral erosion of their edges and its vertical evolution. This last responds to the balance among the sedimentation, erosion, and relative sea level increase (Marani et al., 2011). The lateral erosion of the marsh edges, and consequently the loss of wetlands, was observed in many sites of the world highlighting the important role of waves in driving erosion processes (Downs et al., 1994; Wray et al., 1995; Day et al., 1998; van de Koppel et al., 2005; Wolters et al., 2005; Ravens et al., 2009; Cowart et al., 2010; Fagherazzi et al., 2013; Francalanci et al., 2013; Leonardi and Fagherazzi, 2014; McLoughlin et al., 2015). In addition, the connection between the wave power and the marsh edge retreating can be appreciated in several coastal areas in the world (e.g. Schwimmer, 2001; Marani et al., 2011; Leonardi and Fagherazzi, 2015). It was also documented that waves are able to erode the marsh edge scarp even without a noticeable sea level rise (Fagherazzi et al., 2013; Mariotti and Fagherazzi, 2013).

More than 4000 km of the Argentine coast (from approximately 5000 km of its total length) are being affected by gradual, natural and evident erosive processes (Codignotto et al., 1992; Codignotto and Aguirre, 1993). Kokot (1997) reported an increase in the erosive processes along the coast of Buenos Aires province during the last three decades of the 20th Century. This author linked the enhanced erosion to changes in atmospheric and oceanic processes which seem to be a consequence of climate change. Barros et al. (2000, 2006) found that the western border of the South Atlantic High and the atmospheric circulation over South-eastern South America have slowly shifted towards the south during the last decades. This displacement produces a higher frequency of easterly winds over the Río de la Plata region (SMN, 1992; Simionato et al., 2005; SMN, 2009; Codignotto et al., 2012). The possibility that wind wave heights are actually increasing in the South-eastern South American Continental Shelf was investigated by Dragani et al. (2010) who found that the most significant increase occurred between the 80's and the 90's, and the largest difference between both decades (0.20 m, 9%) was observed to the east of the Río de la Plata mouth (around 34° S 48° W). The wave height increase resulted slightly lower (7%) over the continental shelf and the outer Río de la Plata (Fig. 1). Several works have shown evident changes in the wind wave climate in the World Ocean, for example, Cox and Swail (2001) and Young et al. (2011), among others. In addition, regional changes in the wind wave climate were also investigated in different places of the world as, for example, on the Australian coast (Hemer et al., 2007) and in Central and South America (Izaguirre et al., 2013; Reguero et al., 2013).

The analysis of a long term wind wave simulation (35 year-long) in a single point located at the center of Samborombón Bay (Fig. 1) showed a significant increment of the frequencies of occurrence (+10 and +7 cases/decade, where each wave model output corresponds to a case, four per day) and heights (+0.04 and +0.02 m/decade) of the waves propagating from the E and ESE directions (Codignotto et al., 2012). Numerical simulations support the hypothesis that higher waves from the E and ESE are becoming more frequent in the coastal area of Samborombón Bay and, as a consequence, the edge scarp would be more frequently exposed to higher levels of wave energy, driving to larger erosion (Codignotto et al., 2012).

Erosion in Samborombón Bay is evident and can be easily measurable by means of field surveys, aerial photographs or satellite images. Nevertheless, the magnitude of a possible wave climate change in the coast of the bay is less perceptible and its quantification constitutes precisely the motivation of the present work. Unfortunately wave data records are not available in the bay and, consequently, such an investigation can only be faced by means of numerical simulations using a
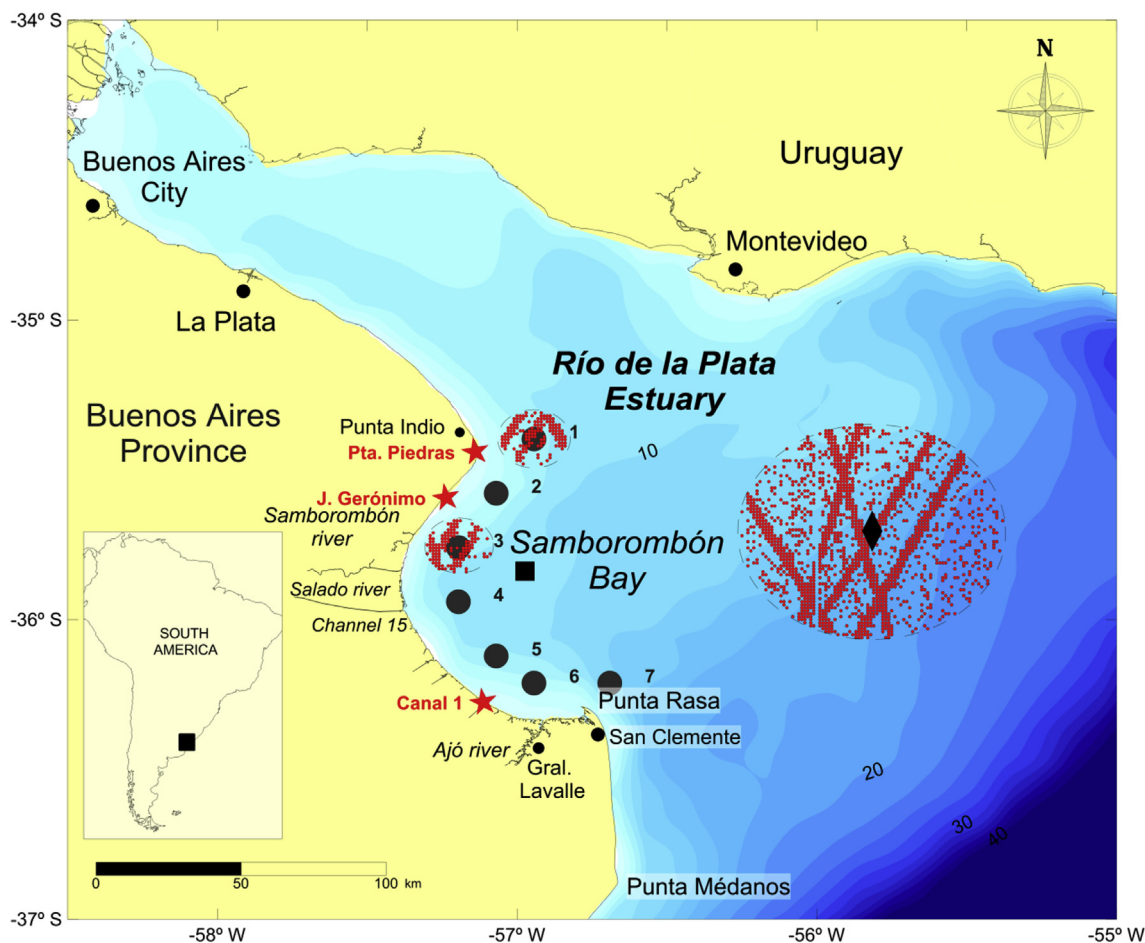

Fig. 1. Río de la Plata Estuary. Satellite wave heights (red dots) within a large circle (radius: 40 km) centered at the Waverider buoy position (black diamond) and within two small circles (radius: 10 km) centered at sites 1 and 3 are presented. Selected sites (black dots) used to describe the wave parameters along the coast are labeled from 1 to 7. The grid node (black square) used by Codignotto et al. (2012) to study the wave climate in the bay is also included. Red stars indicate where the marsh edge retreat was measured. Depth contours in meters. (For interpretation of the references to colour in this figure legend, the reader is referred to the Web version of this article.)

Fig. 2. Typical shoreline at Samborombón bay near site 5. (a) Undercutting of marsh scarp, the rootmat forms an overhang (b) which falls at the foot of the scarp.

regionally validated model. The aim of this paper is to build a realistic coastal wave model for Samborombón Bay, to investigate if the coastal wave parameters are actually changing, and to analyze if the wave climate and its possible change are in agreement with an acceleration of the erosive processes reported in the bay. For this purpose, directional significant wave heights (Hs), frequency of occurrence, and their trends, are simulated at seven sites disposed along the coast of Samborombón Bay (Fig. 2). In addition, the alongshore energy flux is estimated (which is proportional to the amount sediment transported along the coast) and the normal energy flux is computed to analyze its possible link with the retreating of the marsh edge, this last, systematically measured during

several coastal campaigns. Finally, a possible link between the long-term variability of simulated wave parameters and two climatic anomalies, El Niño/Southern Oscillation (ENSO) and Southern Annual Mode (SAM), are investigated and discussed.

2. Study area

The coast of Samborombón Bay (Fig. 1) is approximately 140 km long, its coastal area is a wetland covering 3000 km² which is around 1 m above the mean sea level, and constitutes a typical low-lying area coastal system (Nicholls et al., 2007). This area shelters a variety of

species of crabs, aquatic turtles and migratory birds (Canevari et al., 1999). It was designated as a Ramsar Wetland, reflecting its significance as a habitat for the buff-breasted sandpiper and other threatened species (https://www.ramsar.org/). The bay exhibits an unusually high density of shorebird species, many of which use the bay as a resting point in their seasonal migrations (Martínez-Curci et al., 2015).

The tide regime in Samborombón Bay is mixed, predominantly semidiurnal (Balay, 1955) and the tidal range slightly increases southeastwards, from Punta Piedras (0.70 m) to Punta Rasa (0.80 m) (SHN, 2018). The presence of storm surges in the Río de la Plata was extensively reported. They occur during events characterized by persistent and strong southerlies, which can be also associated with frontal passages. These meteorological conditions produce differences between observed sea level and astronomical tides. When this difference (storm surge) is large, it is known as "*sudestada*" and affects considerable areas of the coast over periods that may extend from some hours to several days. The action of storm surges has been clearly recognized at coastal water of the Río de la Plata (Campetella et al., 2007). The coincidence of large or even moderate high tides and large meteorologically induced surges has historically caused floods and damages in many coastal locations (D'Onofrio et al., 1999, 2008; Pousa et al., 2013). On the other hand, mean sea level trend was estimated in $+1.68 \pm 0.05$ mm/year (period: 1905–2003) in the Río de la Plata (D'Onofrio et al., 2008).

The bottom of Samborombón Bay is mainly composed of fine sediments, especially mud and organic matter (Bértola, 1995). There is not a high resolution bathymetry for Samborombón Bay. There are not depth soundings between the coast and the isobath of 3 m, and depth data density is very scarce between the isobaths of 3 and 5 m (SHN, 1969). The slope of the bottom, between the coast and the isobath of 5 m, is approximately 0.0005. Bottom depth gradually increases offshore, reaching 10 m in the outer area of the bay, between Punta Rasa and Punta Piedras (Fig. 1). The intertidal zone displays a gentle slope and ends in a scarp of less than 1 m high (Fig. 2). Because of its composition of non consolidated very fine sand and silt, it is highly vulnerable to erosion. Breaking waves are typically spilling type at the surf zone (Bértola and Ferrante, 1996) and, although wave measurements are not available in the coastal area, regional numerical simulations suggested that the mean wave height would be lower than 0.5 m in the bay (Dragani et al., 2010). It was suggested that the morphodynamics of the coast essentially responds to the effects of the wave attack on the edge scarp (Codignotto et al., 2012), especially during energetic wave events (Dragani et al., 2013a).

3. Data and methods

Observed and satellite wave parameters gathered at the Río de la Plata mouth were used to validate SWAN (Simulating Waves Nearshore) model. Alongshore and incident wave energy fluxes were estimated from simulated wave parameters in Samborombón Bay. Possible relationships between the inter-annual variability in simulated wave parameters and two climatic indices (ENSO and SAM) were also investigated. Field measurements of the marsh edge retreat at three locations of the bay are also described in this section.

3.1. Wave observation

The single long-term wave directional data series (*Hs*, peak period, and wave direction) in the region was obtained from a Datawell Waverider buoy (Datawell, 1997) moored at 16 m depth (35° 40′ S, 55° 50′ W, Fig. 1) from 1996 to 2006. The instrument was set up to take sea level records of 20 min each, with a 0.5 s sampling interval and every 160 min. Time series have several gaps, one of them longer than one year, three of them eight months long, and six others of various durations (Fig. 3). Satellite wave heights obtained from the following satellite altimeter missions: Topex/Poseidon, Jason1, Jason2, ERS1, ERS2, Envisat, HY-2A and GFO were also used in this work. These

satellite wave heights are available in AVISO Satellite Altimetry database (Archiving, Validation and Interpretation of Satellite Oceanography data) particularly from DT CorSSH (Delayed Time Corrected Sea Surface Height), produced by CLS Space Oceanography Division and the CNES (Center National D' Études Spatiales, Francia). The temporal sampling interval of satellite data is variable because it depends on the orbital period of each satellite mission, which ranges from 9.8 days (Topex and Jason1/2) to 35 days (ERS1/2 and Envisat). Following Durrant et al. (2009), satellite *Hs* were used for complementing the validation of simulated wave parameters (period: 1996–2006). Satellite data inside a circle (radius: 40 km) centered at the Waverider buoy position (3611 data, Fig. 1) were considered. Only satellite data with differences in time lower than $| \pm 1|h$, respect to the buoy acquisition time, were selected for the validation resulting in 378 pairs of observed and satellite *Hs*.

3.2. Wave model

SWAN model was used to simulate significant wave height (*Hs*), peak period (*Tp*) and direction (*α′*) in Samborombón bay. It is a spectral wave (third generation) model that provides realistic estimations of wave parameters in coastal regions (Booij et al., 1999). SWAN model solves the transport equations for wave action density. Default values for model parameters were considered for controlling dissipation by depth-induced wave breaking, dissipation by bottom friction, whitecapping, three wave-wave interaction (triads) and quadruplets.

Surface wind data from NCEP/NCAR Reanalysis I (space resolution 1.875° in longitude and 1.905° in latitude) were used to force the simulations. It has been successfully utilized as forcing in several numerical regional studies in the area (Simionato et al., 2005, 2006a; 2006b, 2007; Dragani et al., 2010; Codignotto et al., 2012). A discussion about the quality of NCEP/NCAR I over the Southern Hemisphere can be found in Simmonds and Keay (2000). A complete description of this reanalysis and its dataset can be found in Kalnay et al. (1996). NCEP/NCAR I properly reproduce the observed wind direction in the Río de la Plata, but it tend to underestimate wind speed, particularly for weak wind conditions (Simionato et al., 2006a,b). Then, a correction factor was applied to the drag coefficient in order to enhance the wave simulations in the outer Río de la Plata (Dragani et al., 2008). The bathymetry data used for the SWAN model was obtained combining a depth data set with 1′ x 1′ resolution taken from GEBCO (2003) charts for the continental shelf and nautical charts (SHN, 1986, 1992, 1999a; 1999b). These data were interpolated to the model grid by applying the method of inverse distance to the second power.

The optimal relationship between the spatial resolution and the model domain extension (model architecture), to simulate waves in the Río de la Plata, was extensively investigated (Dragani et al., 2008). It was found that the best model architecture corresponded to a computational domain extended from 29.747° to 42.203° S, and from 40.405° to 65.418° W, with spatial resolution of 22.7×20.0 km (100×70 grid points). The relatively low spatial resolution of this domain is due, firstly, to the lack of bathymetric data and the low spatial resolution of soundings (depth measurement) in the region and, secondly, to the relatively low spatial resolution of the reanalysis used to drive the simulations. It was noted that if the spatial resolution in the computational domain increases, the simulated wave parameters do not significantly improve. More details about the architecture, implementation, and validation of SWAN model in the study area can be found in Dragani et al. (2008) and Martin et al. (2012).

3.3. Wave model validation

Numerical simulations (1971–2012) were validated using the above mentioned *in-situ* wave parameters and satellite *Hs*. Computed bias (difference between observed and simulated mean values), root mean square error and correlation coefficient between *in-situ* and simulated
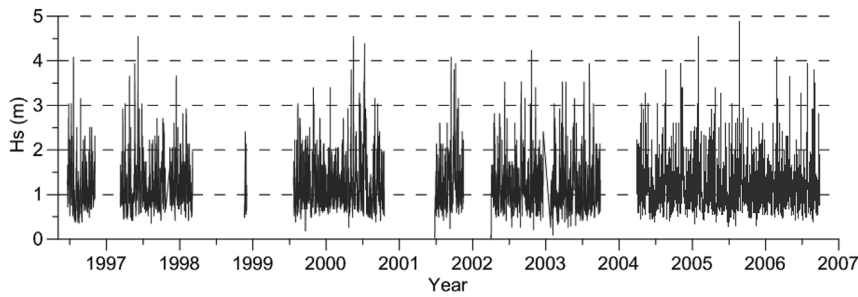
Fig. 3. Performance of Hs acquisition at the Río de la Plata mouth. Gaps correspond to lapses without wave data acquisition.
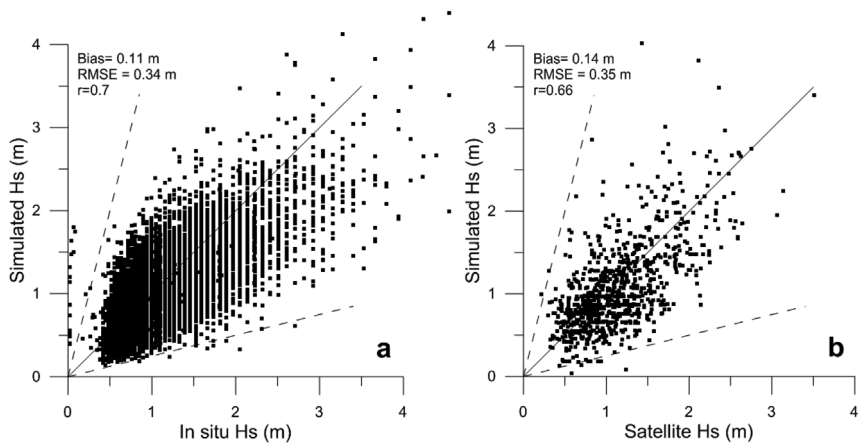

Fig. 4. Scatter plots between simulated and (a) in situ and (b) satellite Hs at the Río de la Plata mouth.

Hs (period: 1996–2006) were +0.11 m, 0.34 m and 0.70, respectively (Fig. 4a). Similar results were obtained between satellite and simulated *Hs* (period: 1991–2008) where bias, root mean square error and correlation coefficient were 0.14 m, 0.35 m and 0.66, respectively (Fig. 4b). Seven sites were selected to study the wave climate. These sites do not necessarily match with the grid nodes of the computational domain. Then, a bi-lineal interpolation was carried out among the four nearest grid nodes to obtain seven sites regularly distributed, located every 20 km along the coast and 15 km offshore (Fig. 1). Comparisons between simulated and satellite wave heights at sites 2 and 4 revealed a spurious overestimation in satellite *Hs* which could be caused by the close distance to the coast. This overestimation is in agreement with Durrant et al. (2009), Gommenginger et al. (2011) and Woolf et al. (2002) who pointed out that the contamination of satellite data caused by the proximity to the coast can produce higher wave heights.

3.4. Longshore wave energy flux

The rate of longshore sediment transport is a very important quantity to be considered in coastal processes. It is proportional to longshore wave energy flux per unit crest (*Pl*), which can be estimated by:

$$Pl = 0.05 \, \rho \, g^{3/2} \, H^{5/2} \, (\cos \alpha)^{1/4} \, (\sin 2\alpha); \, (\text{CERC}, 1984) \quad (1)$$

ρ is the water density (equal to 1022.5 kg m^{-3}, Piola and García, 1993), *g* the acceleration due to gravity (9.86 m s^{-2}), and α the wave angle between the wave crest and the shoreline. The predominant orientation of the shoreline (respect to a geographic parallel) was estimated from Landsat images (Data SIO, NOAA, U.S. Navy, NGA, GEBCO, source: Google Earth, 2018). For example, the predominant orientation of the shoreline is 0° at site 6 (orientation: W-E), 135° at site 5 (NW-SE), and 45° at site 2 (NE-SW). Simulated wave direction ($0 \le \alpha' < 360^0$) indicates where the wave is coming from (0^0 from the north, 90^0 from the east, 180^0 from the south, and so on). In order to properly apply eq.

(1), α' was transformed to give the angle between the direction of wave propagation and the line normal to the coast (α). Values of α equal to zero correspond to normal incidence of waves and, consequently, *Pl* is also equal to zero (eq. (1)). *Pl* can only flow in two possible directions depending on the sign of the instantaneous value of α: rightward (positive) or leftward (negative), respect to an observer located at the coast and looking to the water. Accordingly, annual net *Pl* (*Pl$_N$*, the average of individual rightward and leftward *Pl* in a year) can also flow in rightward or leftward direction.

Deep water wave parameters (*Hs* and α) should be used in eq. (1). Mean *Tp* is lower than 4 s in the Río de la Plata (Dragani et al., 2010) and then the deep water condition is reached relatively near the coast, for depths greater than 12.5 m ($h/L_o > 0.5$, L_o: deep water length wave equal to $(g/2\pi)Tp^2$, and *h*: local depth). It was tested that eq. (1) overestimates *Pl* when is applied with wave parameters corresponding to intermediate water. Greatest difference was obtained at site 2 (27%) but, in general, errors lower than 11% were obtained in the other studied sites.

3.5. Incident wave energy flux

The incident wave energy flux per unit crest (*Pi*) at the breaking line can be computed as:

$$Pi = (\rho \, g \, Hs_b^2 \, Cg_b \, \cos \alpha_b) \, / \, 8; \, (\text{Dean and Dalrymple, 2001}) \quad (2)$$

Hs$_b$ is the breaking wave height, α_b the angle between the direction of wave propagation and a line normal to the coast, and *Cg$_b$* the wave group velocity at the breaking line. If losses or addition of energy are negligible (energy conservation) in the wave propagation from deep/intermediate water to shallow water, eq. (2) can be written as:

$$Pi = (\rho \, g \, Hs^2 \, Cg \, \cos \alpha) \, / \, 8 \quad (3)$$

Hs, α and *Cg* are obtained from the numerical simulation at the sites previously described.

3.6. Hs, Pl_N and Pi trends

Trends in *Hs*, frequency of occurrence, *Pl_N* and *Pi* data series (period: 1971–2012) were estimated using Sen's slope estimator (Sen, 1968) with monthly mean parameters. The significance of the computed trend was tested using the Seasonal Mann–Kendall (SK) trend test (Hirsch et al., 1982; Hirsch and Slack, 1984) with a confidence level of 95%. The SK test accounts the data serial dependence (i.e. the seasonality) by calculating results from the Mann–Kendall (MK) trend test (Kendall, 1955; Mann, 1945) for each month separately and then combining the results. The MK is a nonparametric test for randomness against trend and has been extensively applied in meteorology and oceanography (see, for example, Wang and Swail, 2001; Meccia et al., 2009; Tokinaga and Xie, 2011; Pescio et al., 2015; Stopa et al., 2016).

3.7. Inter-annual variability of simulated Hs

Possible relationships between the inter-annual variability in simulated wave parameters and two climatic anomalies (ENSO and SAM) were also investigated. ENSO cycle refers to the coherent and sometimes very strong year-to-year variations in sea-surface temperatures, convective rainfall, surface air pressure and atmospheric circulation that occur across the equatorial Pacific Ocean, and has global repercussions (http://www.cpc.noaa.gov/products/analysis_monitoring/ensostuff/ensofaq.shtml#NINO). On the other hand, SAM is one of the annular modes of variability and describes the N−S movement of the westerly wind belt which significantly impacts on the South Atlantic Ocean circulation (http://www.bom.gov.au/climate/enso/history/ln-2010-12/SAM-what.shtml). Pearson linear correlation coefficient (*r*) was estimated to investigate if the SOI and SAM indices are related to simulated mean annual *Hs* in the bay.

3.8. Measurements of the marsh edge retreat

Systematic measurements of the cliff retrogression are being carried out at three selected points of the Samborombón Bay coast from January 2010 (Fig. 1). Two points are located at Punta Piedras and Juan Gerónimo Ranch (at the North of the bay) and the other one at Canal 1 (at the central/South sector of the bay). Control points (landmarks with known latitude, longitude and elevation respect to the mean sea level) were fixed very close to the edge of the cliff at each one of the mentioned location. The distances from the landmark to the edge of the cliff were surveyed every two months, approximately. These tasks let to quantify the edge marsh retreat at the Samborombón Bay coast.

4. Results

Simulated and satellite *Hs* trends, estimated *Pl* and *Pi*, a possible relationship between the marsh edge retreat and *Pi* and the Inter-annual variability of simulated *Hs* (and its connection with SAM and SOI indices) are computed in this section.

4.1. Simulated Hs and their trends

Hs data series (1971–2012) were analyzed without considering the wave direction (Table 1). It can be seen that mean *Hs* is quite uniform (0.27–0.30 m) along the coast of the bay (sites 1 to 6), except close to Punta Rasa (site 7) where mean *Hs* is somewhat higher reaching 0.52 m (Fig. 1). Estimated mean *Hs* trends are positive, small and significantly different from zero in sites 1 to 6 (around +0.4 ± 0.2 cm/decade), but at the site 7 the trend is a little higher (+0.8 ± 0.3 cm/decade). Maximum *Hs* was 0.80 m in the northern sector of the bay (site 2) and (1.54 m) close to Punta Rasa (site 7). Simulated *Tp*, typically lower than 4 s, show the prevalence of sea (high-frequency) waves at the coast of the bay. Computed *Hs_99* (the percentile 99th of the *Hs*) are also uniform along the coast of the bay (0.52–0.57 m). Maximum *Hs_99* was also

Table 1
Statistics of non-directional wave parameters, for the simulated period with SWAN model (1971–2012), at the seven sites located along the coast of Samborombón bay.

Site	Hs (m)	Hs trend (cm/decade)	Hs_99 (m)	Hs_99 trend (cm/decade)	Hs-max (m)	Tp (s)
1	0.27	+0.5	0.52	+0.6	0.62	2.0
2	0.29	+0.5	0.58	+0.8	0.80	2.1
3	0.26	+0.4	0.52	+0.8	0.66	2.0
4	0.26	+0.4	0.50	+0.7	0.62	1.9
5	0.29	+0.4	0.55	+0.6	0.73	2.0
6	0.30	+0.4	0.57	+0.6	0.75	2.0
7	0.52	+0.8	1.07	+1.4	1.54	3.0

obtained at site 7 (1.07 m). Computed *Hs_99* trends are also positive and significantly different from zero along the coast of the bay (around +0.7 ± 0.4 cm/decade). Maximum *Hs_99* trend was obtained at site 7 (+1.4 ± 0.8 cm/decade).

Subsequently, a directional analysis considering the eight main wave propagation directions was carried out. The N direction (0°) includes all the cases of waves propagating from directions between 337.5° and 22.5°, the NE direction (45°) between 22.5° and 67.5°, the E direction (90°) between 67.5° and 112.5°, and so on. It was obtained that NE is the most frequent direction of propagation in Samborombón Bay, with a number of cases (frequency of occurrence) ranged from 19.4 to 23.7%. The occurrences were around 15% for the E and N directions, and somewhat lower (13%) for the SE direction. S, SW, W and NW directions present occurrences lower than 10%. Wave roses were built for each studied site (1–7). As an example, only sites 1, 4 and 7 are described in this paper which represent the sectors north, central and south of the bay, respectively (Fig. 5). In the northern sector of Samborombón Bay (site 1), the most frequent wave propagation directions are from NE (21.1%), E (16.4%), N (15.4%) and SE (13.1%) which are characterized by *Hs* between 0.20 and 0.30 m, and *Tp* between 1.2 and 1.4 s. In the central sector of the bay (site 4), the most frequent wave propagation directions are from NE (21.5%), N (16.3%), E (15.9%) and SE (11.6%) with *Hs* and *Tp* between 0.30 and 0.40 m, and 1.4 and 1.7 s, respectively. At the south of the bay, close to Punta Rasa (site 7), the most frequent propagation directions are NE (23.6%), N (16.7%), E (15.4%) and SE (11.2%) with *Hs* and *Tp* between 0.30 and 0.70 m, and 2 and 2.5 s, respectively. The S, SW, W and NW directions have occurrence frequencies lower than 10%, and mean *Hs* and *Tp* somewhat lower than the mentioned values corresponding to the main propagation directions for the three analyzed sites.

Highest *Hs* trends (around +1 cm/decade) were observed in the central and southern sectors of the bay (between site 4 and 7) for the E and NE directions. Maximum trends for directions E and NE were obtained at the site 7 (+1.2 ± 0.7 cm/decade, i.e. for NE +2.1 ± 1.2% per decade respect to mean *Hs*, this last equal to 0.57 m). Maximum trends in the frequencies of occurrence (number of cases) were found for the direction E at sites 3 and 4 (+17 ± 7 cases/decade), and for the direction NE at the site 3 (+15 ± 8 cases/decade). On the contrary, the frequencies of occurrence for waves coming from the W, NW and N presented a significant reduction of around −15 ± 6 cases/decade.

4.2. Satellite Hs trends

Hs trend was computed from satellite data series gathered at the Río de la Plata mouth (mean *Hs*: 1.1 m) resulting +6.4 ± 5.5 cm/decade (period: 1992–2012). This constitutes an increasing of 6% per decade respect to the mean *Hs* (Fig. 6). It can be seen than relative satellite *Hs* trend computed at the mouth of the Río de la Plata is around three times higher than the *Hs* trend computed at site 3 (6% *vs* 1.7%). This higher trend obtained in the Río de la Plata mouth can be explained
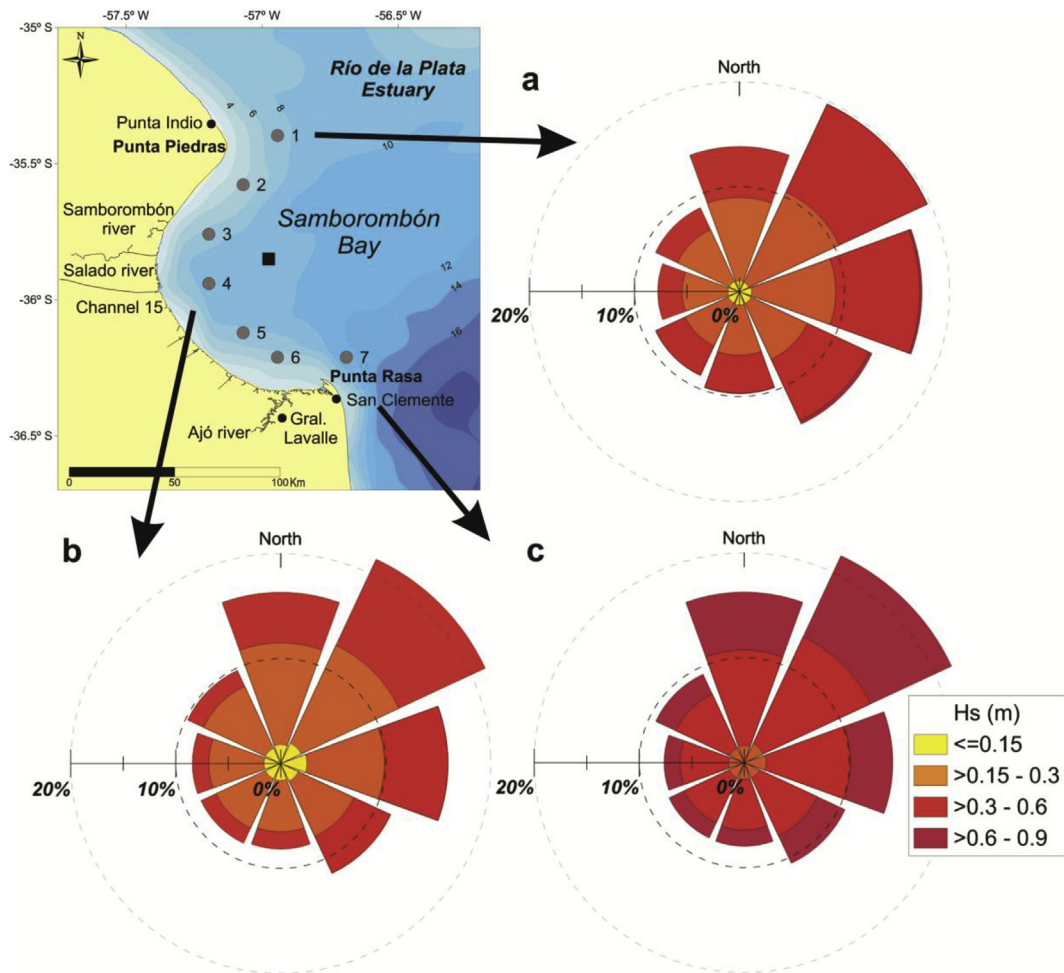
Fig. 5. Directional wave roses at sites 1 (a), 4 (b) and 7 (c).

because this site is located more than 100 km from the coast, in a deeper area of the estuary (20 m).

4.3. Wave energy fluxes

Computed Pl_N resulted very low in Samborombón Bay, reaching a minimum value at the site 4 (+3.9 J/ms), and flow predominantly southwards from site 2 to 5. On the contrary, Pl_N flows clearly towards the center of the bay (northwestwards) reaching a maximum value at site 6 (−30.2 J/ms). Therefore numerical results suggest a convergence of Pl_N between the sites 5 and 6 (Fig. 7). Computed Pl_N trends resulted significantly different from zero only at site 6 (−4.7 J/ms/decade or −4.3% per decade) indicating that northwestwards flux would be

accentuating in time.

Estimated Pi is one magnitude order greater than Pl_N and is quite homogeneous along the coast of Samborombón Bay. It is around 80–90 J/ms between sites 2 and 4 and increases a little at sites 5 (115.9 J/ms) and 6 (126.1 J/ms). Computed Pi trends resulted positive and significantly different from zero at all sites. Relative trends of Pi are around +5%/decade between the sites 2 and 5, and decrease a little at site 6 (+1.8%/decade).

4.4. Marsh edge retreat vs Pi

Marsh edge retreat presented different annual mean rates at the three control points. The annual mean marsh edge retreat is 1.26 m/
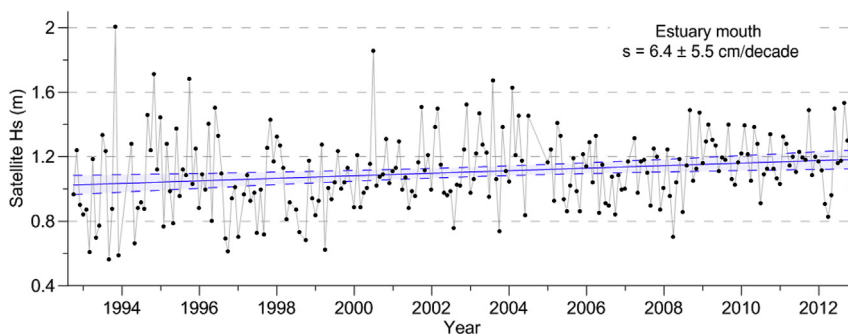

Fig. 6. Data series of monthly mean satellite heights at the Waverider location (Fig. 1). Estimated trend line (blue solid line) and its uncertainty (± 95%, blue dashed line) are also shown. (For interpretation of the references to colour in this figure legend, the reader is referred to the Web version of this article.)
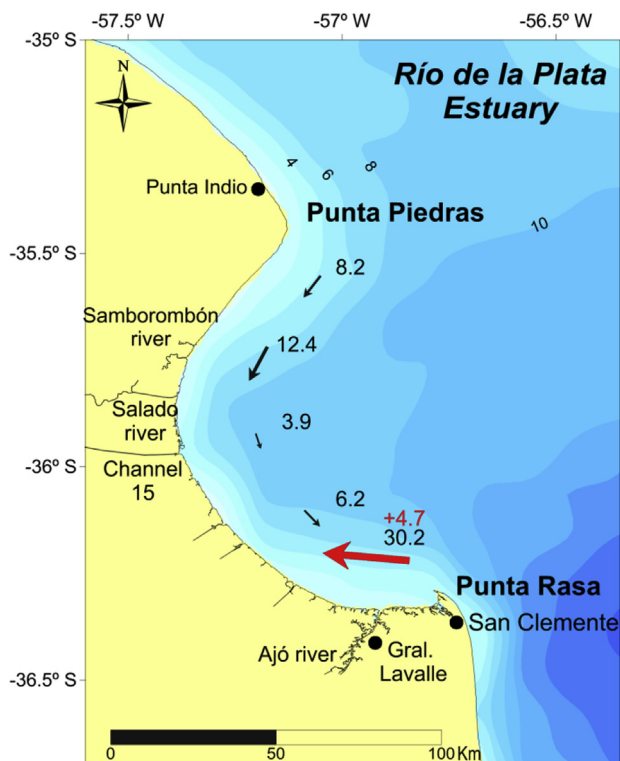
Fig. 7. Averaged annual Pl_N. Arrows indicate direction and intensity (J/ms) of Pl_N. The single site where the computed Pl_N trend was significantly different from zero (95%) is indicated with a red arrow and the value of the trend (J/ms/decade) is also indicated in red. Contours in meters. (For interpretation of the references to colour in this figure legend, the reader is referred to the Web version of this article.)

Fig. 8. Cumulative marsh edge retreat *vs* the integrated incident wave energy flux (Pi) at three monitored locations (2010–2012). Corresponding least-square regression lines are included. Coefficients of determination (R^2) are also indicated.

year at J. Gerónimo Ranch and is slower at Punta Piedras (0.38 m/year) because the sediments of the marsh edge are a little more consolidated (Fig. 1). The total marsh edge retreat (respect to its initial position) and the integrated or accumulated value of the *Pi* (for the same period) were computed. Scatter plots between both quantities are presented for the three monitored coastal locations (Fig. 8). It can be seen that the total edge retreat is directly proportional to the integrated *Pi*. The relationship between the total edge retreat and the integrated *Pi* is similar in both locations surveyed at the north of the bay (Punta Piedras and J. Gerónimo Ranch, Fig. 1), presenting high coefficients of determination (R^2), between 0.91 and 0.94 (Fig. 8). On the contrary, R^2 is lower (0.61, Fig. 8) at the Central/south location of the bay (Canal 1, Fig. 1). Between March 3 and April 7, 2010, a storm surge event affected the southern area of the bay. As a consequence, a very significant edge marsh retreat was measured in Canal 1, which is clearly represented by the difference (1.25 m) between the first and second data points of the scatter plot (Fig. 8). During this storm surge event, the water level was probably close to the marsh edge platform elevation during several hours and, consequently, the waves attacked more efficiently the scarp. This abrupt jump of 1.25 m between the first and the second data point would produce the lower value of R^2 estimated for Canal 1.

4.5. Inter-annual variability of simulated Hs

Pearson linear coefficient (*r*) between simulated (no directional) mean annual *Hs* and SAM and SOI indices were computed. Values of *r* lower than 0.25 were obtained at the seven studied sites. Subsequently, *r* were calculated between frequencies of occurrence (for all directions) and both climatic indices. Positive *r* (around 0.35–0.45, significantly different from zero) were obtained between SOI index and frequencies of occurrence for the NE direction in all sites (Fig. 9a). Similarly,
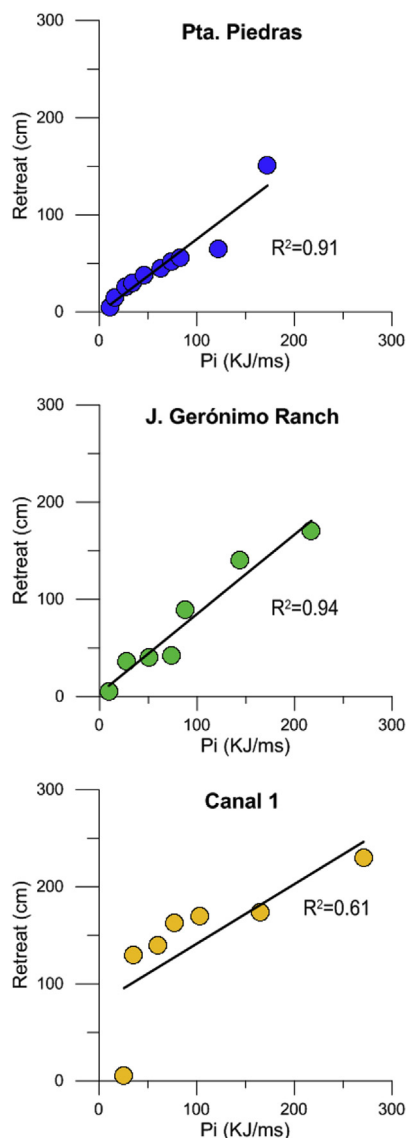
positive *r* (0.40–0.50) were obtained between SAM index and frequencies for the same direction (Fig. 9b). On the contrary, negative *r* (significantly different from zero) were obtained between both climatic indices and frequencies of occurrence for N and W directions (approximately −0.4). The rest of the analyzed directions presented values of *r* between ± 0.25 (significantly no different from zero).

An analysis was carried out to explore if *Hs* variability (for N and NE directions) can be linked to SOI index magnitude. Following to Jin et al. (2005) SOI can be classified into five groups according to their magnitude, such as "strong El Niño" (SOI < −2), "weak El Niño" (−2 ≤ SOI < −1), "normal condition" (−1 ≤ SOI ≤ 1), "weak La Niña" (1 < SOI ≤ 2), and "strong La Niña" (SOI > 2). Significant *Hs* trends for NE and E directions (+1.6 and + 1.9 cm/decade, respectively) and frequencies of occurrence for N and NW directions (−4 and −2 cases/decade) were obtained when only strong and weak El Niño events were considered. In addition, significant *Hs* trends for NE direction (+1 cm/decade) and frequencies of occurrence for N and NW directions (- 2.6 and −1.6 cases/decade) were obtained when only strong and weak La Niña events were taken into account. Wave
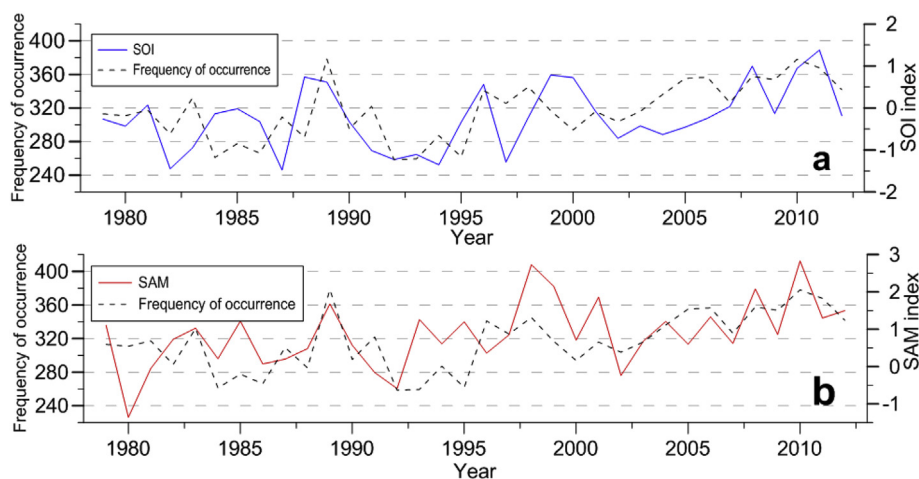
Fig. 9. NE annual frequency of occurrence *vs.* (a) annual SOI index and (b) SAM index.

parameters were also analyzed along the Samborombón Bay coast during two strong El Niño events (Huang et al., 2016; Santoso et al., 2017). *Hs* was approximately 7% higher than the annual mean *Hs*, and the frequencies of occurrence were 30% and 42% greater than the mean values for NE and E directions, respectively, and 40% and 50% lower for W and NW directions, respectively, for the 1997–1998 El Niño event. On the other hand, the frequency of occurrence was greater than 55% for the NE direction and lower than 64% for the W direction, respect to the annual mean values, for the 1982–1983 El Niño event.

5. Discussion

Dragani et al. (2013b) found that the most energetic sea conditions propagate predominantly from the SE in the Río de la Plata mouth. Previously, it was also suggested that the coast of Samborombón Bay is partially protected from waves propagating from the SE, being the northern sector of the bay the area more vulnerable to waves coming from SE (Dragani and Romero, 2004). In this regard, numerical simulations carried out in this work suggest that waves propagating from the SE are a little more frequent at the north of the bay (13.1% at site 1) in comparison with the central and southern sector of the bay (approximately 11%). Codignotto et al. (2012) suggested that the morphodynamics of the coast of Samborombón Bay essentially responds to the effects of the wave attack on the edge scarp. The shoreline of Samborombón Bay is characterized by a vertical scarp, which exposes the rootmat and the underlying muds (Fig. 2). The erosion mechanism in this kind of environments was described by Schwimmer (2001). The relatively unconsolidated muds erode faster than the overlying rootmat and, as a result, the rootmat commonly forms an overhang which falls at the foot of the scarp (Fig. 2). Fine sediments are mainly incorporated into the aquatic system and the scarp moves back (retrogression). Systematic measurements of the edge scarp position indicate that the mean regression is approximately 1 m per year in Samborombón Bay (Codignotto et al., 2012). This mechanism of natural erosion, clearly observable from the coast, is well-matched with the wave climate obtained from numerical simulations, which is characterized by waves predominantly propagating from N, NE, E and SE.

The analysis of the 42 year-long simulation shows maximum trends in *Hs* for directions E and NE at the site 7 (+1.2 ± 0.7 cm/decade). Maximum trends in the frequencies of occurrence were also found for the direction E at sites 3 and 4 (+17 ± 7 cases/decade) and for the direction NE at the site 3 (+15 ± 8 cases/decade). Therefore, the numerical simulations show that highest waves, propagating from the E and NE, are becoming more frequent in the coastal area of Samborombón Bay. As a consequence, the edge scarp would be more frequently exposed to higher levels of wave energy, driving to larger

erosion. This is in agreement with Codignotto et al. (2012) who noted acceleration in the erosive processes of the bay which was associated with positive trends of *Hs* and frequency of waves propagating from E and ESE. However, the latter was inferred from simulated wave parameters obtained at a single node of SWAN model located in the center of the bay (Fig. 2). In this work, the wave analysis was carried out from wave parameters simulated along the coast of the bay (sites 1 to 7). On the contrary, it was obtained that maximum trends in *Hs* and frequency of occurrence correspond to E/NE directions.

From annual frequencies of occurrence for NE direction and SOI and SAM indices it can be seen that the frequencies of occurrence present a remarkable inter-annual variability which ranges from 260 (1984) to 380 (1989) cases per year (Fig. 9). In general, frequency of occurrence and SOI index data series present a good agreement. The most noticeable differences can be seen in 1983, 1987 and 2000 (Fig. 9a). Frequency of occurrence and SAM index data series also match reasonably well. In this case the main differences can be appreciated between 1993 and 1995 (Fig. 9b). Particularly, during two strong El Niño events *Hs* was significantly higher than the annual mean *Hs*, the frequencies of occurrence for NE and E directions were 30–50% greater than the mean values, and 40–60% lower for W and NW directions. Results show that both climatic anomalies (ENSO and SAM) would mildly impact on the wave climate in Samborombón Bay. Then, although discussed trends (in *Hs*, frequency of occurrence, *Pl_N* and *Pi*) were estimated from relatively long data series (42 years) it should be noticed that the presence of both climatic anomalies can slightly impact on them.

On the other hand, numerical simulations suggest the presence of a convergent pattern of *Pl_N* between the sites 5 and 6 (Fig. 7). This convergence could play a certain role in the relocation of eroded sediment in the bay. Nevertheless, visual inspections carried out during several coastal campaigns did not reveal the presence of accumulated materials in this sector. This could be explained because the intensity of the maximum mean annual *Pl_N* is very low in the bay (30.2 J/ms). For instance, *Pl_N* estimated near Mar del Plata, located in the southern coast of Buenos Aires Province, is around 2150 J/ms (Perez et al., 2017) and produces a northward net sediment transport of $3.9105 \, m^3 \, yr^{-1}$ (Caviglia et al., 1991). Then, it can be clearly seen that the maximum *Pl_N* intensity estimated in Samborombón Bay is almost three orders of magnitude lower than *Pl_N* computed in Mar del Plata. In addition, it is important to highlight that as *Pl* was computed with wave parameters corresponding to intermediate water and then, as was previously explained, *Pl* could be overestimated around 11% (maximum overestimation was estimated at site 2, 27%). It could be speculated that the speed of the longshore currents would be very low in Samborombón Bay and then the alongshore transport is mainly dominated by tide, which would explain the absence of accumulated sediment between the

sites 5 and 6.

The mean annual marsh edge retreats estimated in this work are of the same order of magnitude that other rates inferred by different authors in the region (Bértola, 1995; Cellone et al., 2016; Codignotto et al., 2012; Pratolongo et al., 2013). Numerical simulations carried out in the present paper showed that *Pi* is around 80–90 J/ms at the northern and central sites of the bay and increases towards the south. A linear relationship between the marsh edge retreat and *Pi* was found for Samborombón Bay. This last is in agreement with some results obtained in other places of the world. For example, Schwimmer (2001) quantified the marsh boundary retreat in Rehoboth Bay, Delaware, United States and obtained an empirical time-averaged erosion rate as function of wave power. Marani et al. (2011) investigated the complex problem of the margin lateral erosion in Venice lagoon (Italy) and found a lineal relationship between the rate of volumetric margin retreat and the mean annual wave power density. Based on a large data set of salt marsh lateral erosion rates collected around the world Leonardi et al. (2015) determined the general response of salt marsh boundaries to wave action. They combined *Pi* and marsh edge retreat data from eight different locations in the United States, Australia and Italy and showed that data collapsed into a unique linear relationship.

6. Conclusions

Numerical simulations show that *Hs* increases southwards, from Punta Piedras (site 1) to Punta Rasa (site 7), and reveal that the main propagation wave directions are from NE, E and N. Maximum *Hs* trend were obtained in the central and southern sector of the bay (E and NE directions). The highest positive trend frequency of occurrence (number of cases) was obtained for the E direction. On the contrary, the frequencies of occurrence for the W, NW and N directions show a significantly decreasing.

Positive *r* (Pearson linear correlation coefficient) were obtained between two climatic indices (ENSO and SAM) and the frequencies of occurrence of waves coming from NE. On the contrary, negative *r* were obtained between both climatic anomalies and the frequencies of occurrence for N and W directions. It was pointed out that the presence of both climatic anomalies can slightly impact on the assessment of trends.

Pi is quite homogeneous along the coast of the bay and one magnitude order greater than *Pl$_N$*. A linear relationship between the marsh edge retreat and *Pi* was found for three selected points of the bay, which is in agreement with some results obtained in other places of the world. *Pi* trends resulted positive and significantly different from zero at all sites. Even though it is clear that the complex coastal processes in the bay are driving by tides, winds (storm surge), mean sea level rise and waves, the results obtained in this paper seem to support that the waves and their changes constitute a very important erosive agent. As a consequence, the edge scarp is more frequently exposed to higher levels of wave energy (*Pi*), driving to larger erosion.

References

D'Onofrio, E., Fiore, M.M.E., Romero, S.I., 1999. Return periods of extreme water levels estimated for some vulnerable areas of Buenos Aires. J. Coast Res. 19, 1681–1693. https://doi.org/10.1016/S0278-4343(98)00115-0.

D'Onofrio, E., Fiore, M., Pousa, J.L., 2008. Changes in the regime of storm surges in Buenos Aires, Argentina. J. Coast Res. 24 (1A), 260–265. https://doi.org/10.2112/05-0588.1.

Balay, M., 1955. La determinación del nivel medio del Mar Argentino, influencias de las oscilaciones del mar no causadas por la marea. Dir. Gral. de Nav. Hidrog., Min. de Marina, pp. 46.

Barros, V.R., Castaneda, M.E., Doyle, M.E., 2000. Recent precipitation trends in southern south America east of the andes: an indication of climatic variability. In: Smolka, P., Volkheimer, W. (Eds.), Southern Hemisphere Paleo- and Neoclimates: Key Sites, Methods, Data and Models, pp. 187–206. https://doi.org/10.1007/978-3-642-59694-0_13. Berlin, Heidelberg.

Barros, V., Menéndez, A., Natenzon, C., Kokot, R., Codignotto, J., Re, M., Bronstein, P., Camilloni, I., Ludueña, S., González, S.G., Ríos, D.M., 2006. Vulnerability to floods in the metropolitan region of Buenos Aires under future climate change. AIACC Working 1–36.

Bértola, G.R., 1995. Geomorfología y sedimentología de los ambientes mareales de la bahía Samborombón, Provincia de Buenos Aires, Argentina. Tesis doctoral. Universidad Nacional de La Plata. Universidad Nacional de La Plata.

Bértola, G., Ferrante, A., 1996. Dinámica y transporte en un canal de marea de la bahía Samborombón. Thalassas 107–119.

Booij, N., Ris, R.C., Holthuijsen, L.H., 1999. A third-generation wave model for coastal regions. Part 1. Model description and validation. J. Geophys. Res. 104 (C4), 7649–7666. https://doi.org/10.1029/98JC02622.

Campetella, C.M., D'Onofrio, E.E., Cerne, B.S., Fiore, M.M.E., Possia, N., 2007. Negative storm surges in the port of Buenos Aires. Int. J. Climatol. 27, 1091–1101. https://doi.org/10.1002/joc.1452.

Canevari, P., Blanco, D.E., Bucher, E.H., 1999. Los beneficios de los humedales de la Argentina. Amenazas y propuestas de soluciones. Wetlands International, Buenos Aires, Argentina, pp. 64.

Caviglia, F.J., Pousa, J.L., Lanfredi, N.W., 1991. A determination of the energy flux constant from the dredge records. J. Coast Res. 7, 543–549.

Cellone, F., Carol, E., Tosi, L., 2016. Coastal erosion and loss of wetlands in the middle Río de la Plata estuary (Argentina). Appl. Geogr. 76, 37–48. https://doi.org/10.1016/j.apgeog.2016.09.014.

Codignotto, J.O., Aguirre, M., 1993. Coastal evolution, changes in sea level and molluscan fauna in the Late Quaternary. Mar. Geol. 110, 163–175. https://doi.org/10.1016/0025-3227(93)90112-9.

Codignotto, J.O., Kokot, R., Marcomini, S., 1992. Neotectonism and Sea-Level-Changes in the coastal zone of Argentina. J. Coast Res. 8, 125–133.

Codignotto, J.O., Dragani, W.C., Martin, P.B., Simionato, C.G., Medina, R. a., Alonso, G., 2012. Wind-wave climate change and increasing erosion in the outer Río de la Plata, Argentina. Cont. Shelf Res. 38, 110–116. https://doi.org/10.1016/j.csr.2012.03.013.

Cowart, L., Walsh, J.P., Corbett, D.R., 2010. Analyzing estuarine shoreline change: a case study of cedar island, North Carolina. J. Coast Res. 26, 817–830. https://doi.org/10.2112/JCOASTRES-D-09-00117.1.

Cox, A.T., Swail, V.R., 2001. A global wave hindcast over the period 1958–1997: validation and climate assessment. J. Geophys. Res. 106, 2313. https://doi.org/10.1029/2001JC000301.

Datawell, 1997. Manual for the Waverider. Laboratory for Instrumentation, LM Haarlem, The Netherlands, pp. 113.

Day, J.W., Scarton, F., Rismondo, A., Are, D., 1998. Rapid deterioration of a salt marsh in Venice lagoon, Italy. J. Coast Res. 14, 583–590.

Dean, R.G., Dalrymple, R.A., 2001. Coastal Processes with Engineering Applications. Cambridge University Press, Cambridge. https://doi.org/10.1017/CBO9780511754500.

Downs, L.L., Nicholls, R.J., Leatherman, S.P., Downst, L.L., Nichollst, R.J., Leathermant, S.P., Hautzenrodert, J., 1994. Coastal of fall historic evolution of a marsh island: bloodsworth Island, Maryland. J. Coast Res. 10, 1031–1044.

Dragani, W.C., Romero, S.I., 2004. Impact of a possible local wind change on the wave climate in the upper Río de la Plata. Int. J. Climatol. 24, 1149–1157. https://doi.org/10.1002/joc.1049.

Dragani, W.C., Garavento, E., Simionato, C.G., Nuñez, M.N., Martin, P., Campos, M.I., 2008. Wave simulation in the outer Río de la Plata estuary: evaluation of SWAN model. J. Waterw. Port, Coast. Ocean Eng. 134, 299–305. https://doi.org/10.1061/(ASCE)0733-950X. 2008)134:5(299).

Dragani, W.C., Martin, P.B., Simionato, C.G., Campos, M.I., 2010. Are wind wave heights increasing in south-eastern south American continental shelf between 32°S and 40°S? Cont. Shelf Res. 30, 481–490. https://doi.org/10.1016/j.csr.2010.01.002.

Dragani, W.C., Martin, P.B., Alonso, G., Codignotto, J.O., Prario, B.E., Bacino, G., 2013a. Wind wave climate change: impacts on the littoral processes at the Northern Buenos Aires Province Coast, Argentina. Climatic Change 121, 649–660. https://doi.org/10.1007/s10584-013-0928-8.

Dragani, W.C., Cerne, B.S., Campetella, C.M., Possia, N.E., Campos, M.I., 2013b. Synoptic patterns associated with the highest wind-waves at the mouth of the Río de la Plata estuary. Dyn. Atmos. Oceans 61–62, 1–13. https://doi.org/10.1016/j.dynatmoce.2013.02.001.

Durrant, T.H., Greenslade, D.J.M., Simmonds, I., 2009. Validation of Jason-1 and Envisat remotely sensed wave heights. J. Atmos. Ocean. Technol. 26, 123–134. https://doi.org/10.1175/2008JTECHO598.1.

Fagherazzi, S., Mariotti, G., Wiberg, P.L., 2013. Marsh collapse does not require sea level rise. Oceanography 26, 70–77. https://doi.org/10.5670/oceanog.2013.47.

Francalanci, S., Bendoni, M., Rinaldi, M., Solari, L., 2013. Ecomorphodynamic evolution of salt marshes: experimental observations of bank retreat processes. Geomorphology 195, 53–65. https://doi.org/10.1016/j.geomorph.2013.04.026.

GEBCO, 2003. User guide to the centenary edition of the GEBCO Digital Atlas and its data sets. In: Jones, M.T. (Ed.), Natural Environment Research Council. Natural Environment Research Council.

Gommenginger, C., Thibaut, P., Fenoglio-Marc, L., Quartly, G., Deng, X., Gómez-Enri, J., Challenor, P., Gao, Y., 2011. Retracking altimeter waveforms near the coasts. In: Vignudelli, S., Kostianoy, A.G., Cipollini, P., Benveniste, J. (Eds.), Coastal Altimetry, pp. 61–75. https://doi.org/10.1007/978-3-642-12796-0_4.

Google Earth, 2018. https://earth.google.com/web.

Hemer, M., Church, J., Hunter, J., 2007. Waves and climate change on the Australian coast. J. Coastal Res. SI 432–437.

Hirsch, R.M., Slack, J.R., 1984. A nonparametric test for seasonal data with serial dependence. Water Resour. Res. 20, 727–732.

Hirsch, R.M., Slack, J.R., Smith, R.A., 1982. Techniques of trend analysis for monthly water quality data. Water Resour. Res. 18, 107–121.

Huang, B., Heureux, M.L., Hu, Z., Zhang, H., 2016. Ranking the strongest ENSO events while incorporating SST uncertainty. Geophys. Res. Lett. 43, 9165–9172. https://doi.org/10.1002/2016GL070888.Received.

Izaguirre, C., Méndez, F.J., Espejo, A., Losada, I.J., Reguero, B.G., 2013. Extreme wave climate changes in Central-South America. Climate Change 277–290. https://doi.org/10.1007/s10584-013-0712-9.

Jin, Y.-H., Kawamura, A., Jinno, K., Berndtsson, R., 2005. Quantitave relationship between SOI and observed precipitation in southern Korea and Japan y nonparametric approaches. J. Hidrol. 301, 54–65. https://doi.org/10.1016/j.jhydrol.2004.06.026.

Kalnay, E., Kanamitsu, M., Kistler, R., Collins, W., Deaven, D., Gandin, L., Iredell, M., Saha, S., White, G., Woollen, J., Zhu, Y., Chelliah, M., Ebisuzaki, W., Higgins, W., Janowiak, J., Mo, K.C., Ropelewski, C., Wang, J., Leetmaa, A., Reynolds, R., Jenne, R., Joseph, D., 1996. The NCEP/NCAR 40-year reanalysis project. Bull. Am. Meteorol. Soc. 77, 437–471.

Kendall, M., 1955. Rank correlation methods. In: Charles Griffin Book Series, pp. 196 London.

Kokot, R., 1997. Littoral drift, evolution and management in Punta Médanos, Argentina. J. Coastal Res. 13, 192–197.

Leonardi, N., Fagherazzi, S., 2014. How waves shape salt marshes? Geology 42, 887–890. https://doi.org/10.1130/G35751.1.

Leonardi, N., Fagherazzi, S., 2015. Effect of local variability in erosional resistance on large-scale morphodynamic response of salt marshes to wind waves and extreme events. Geophys. Res. Lett. 42, 5872–5879. https://doi.org/10.1002/2015GL064730.

Leonardi, N., Ganju, N.K., Fagherazzi, S., 2015. A linear relationship between wave power and erosion determines salt-marsh resilience to violent storms and hurricanes. Proc. Natl. Acad. Sci. Unit. States Am. 113 (1), 64–68. https://doi.org/10.1073/pnas.1510095112.

Mann, H.B., 1945. Non-parametric tests against trend. Econometrica 13, 245–259.

Marani, M., D'Alpaos, A., Lanzoni, S., Santalucia, M., 2011. Understanding and predicting wave erosion of marsh edges. Geophys. Res. Lett. 38, 1–5. https://doi.org/10.1029/2011GL048995.

Mariotti, G., Fagherazzi, S., 2013. Critical width of tidal flats triggers marsh collapse in the absence of sea-level rise. Proc. Natl. Acad. Sci. U.S.A. 110, 5353–5356. https://doi.org/10.1073/pnas.1219600110.

Martin, P., Dragani, W., Cerne, B., Alonso, G., Pescio, A., Prario, B., 2012. Numerical simulation of wind waves on the Río de la Plata: evaluation of four global atmospheric databases. Braz. J. Oceanogr. 60, 501–511. https://doi.org/10.1590/S1679-87592012000400008.

Martínez-Curci, N.S., Isacch, J.P., Azpiroz, A.B., 2015. Shorebird seasonal abundance and habitat-use patterns in Punta Rasa, Samborombón bay, Argentina. Waterbirds 38, 68–76. https://doi.org/10.1675/063.038.0109.

McLoughlin, S.M., Wiberg, P.L., Safak, I., McGlathery, K.J., 2015. Rates and forcing of marsh edge erosion in a shallow coastal bay. Estuar. Coasts 38, 620–638. https://doi.org/10.1007/s12237-014-9841-2.

Meccia, V.L., Simionato, C.G., Fiore, M.E., D'Onofrio, E.E., Dragani, W.C., 2009. Sea surface height variability in the Rio de la Plata estuary from synoptic to inter-annual scales: results of numerical simulations. Estuar. Coast Shelf Sci. 85, 327–343. https://doi.org/10.1016/j.ecss.2009.08.024.

Nicholls, R.J., 2011. Planning for the impacts of sea level rise. Oceanography 24, 144–157. https://doi.org/10.5670/oceanog.2011.34.

Nicholls, R.J., Wong, P.P., Burket, V.R., Codignotto, J.O., Hay, J.E., McLean, R.F., Ragoonaden, S., Woodroffe, C.D., 2007. Coastal systems and low-lying areas. In: Parry, M.L., Canziani, O.F., Palutikof, J.P., van der Linden, P.J., Hanson, C.E. (Eds.), Climate Change 2007: Impacts, Adaptation and Vulnerability. Contribution of Working Group II to the Fourth Assessment Report of the Intergovernmental Panel on Climate Change. Cambridge University Press, Cambridge, UK, pp. 315–356.

Perez, I., Alonso, G., Pescio, A., Dragani, W., Codignotto, J., 2017. Longshore wave energy flux: variability and trends in the southern coast of Buenos Aires, Argentina. Regional Studies in Marine Science 16, 116–123. https://doi.org/10.1016/j.rsma.2017.08.002.

Pescio, A.E., Martin, P.B., Dragani, W.C., 2015. Wind speed trends over the southwestern Atlantic Ocean, between 33° and 50°S. Int. J. Climatol. https://doi.org/10.1002/joc.4348.

Piola, A.R., García, O.A., 1993. Publicación H-670. Atlas oceanográfico de la cuenca Argentina Occidental y de la plataforma continental lindera. Ciudad de Buenos Aires, pp. 267.

Pousa, J.L., D'Onofrio, E.E., Fiore, M.M.E., Kruse, E.E., 2013. Environmental impacts and simultaneity of positive and negative storm surges on the coast of the Province of Buenos Aires, Argentina. Environ. Earth Sci. 68, 2325–2335. https://doi.org/10.1007/s12665-012-1911-9.

Pratolongo, P., Mazzon, C., Zapperi, G., Piovan, M.J., Brinson, M.M., 2013. Land cover changes in tidal salt marshes of the Bahía Blanca estuary (Argentina) during the past 40 years. Estuar. Coast Shelf Sci. 133, 23–31. https://doi.org/10.1016/j.ecss.2013.

07.016.

Ravens, T.M., Thomas, R.C., Roberts, K. a., Santschi, P.H., 2009. Causes of salt marsh erosion in Galveston Bay, Texas. J. Coast Res. 252, 265–272. https://doi.org/10.2112/07-0942.1.

Reguero, B.G., Méndez, F.J., Losada, I.J., 2013. Variability of multivariate wave climate in Latin America and the Caribbean. Glob. Planet. Chang. 100, 70–84. https://doi.org/10.1016/j.gloplacha.2012.09.005.

Santoso, A., Mcphaden, M.J., Cai, W., 2017. The defining characteristics of ENSO extremes and the strong 2015/2016 El Niño. Rev. Geophys. 55, 1079–1129. https://doi.org/10.1002/2017RG000560.

Schwimmer, R., 2001. Rates and processes of marsh shoreline erosion in Rehoboth Bay, Delaware, USA. J. Coast Res. 17, 672–683. https://doi.org/10.2307/4300218.

Sen, P.K., 1968. Estimates of regression coefficient based on Kendall's Tau. J. Am. Stat. Assoc. 63, 1379–1389.

SHN, 1969. Bahía Samborombón, Carta Náutica H115, first ed. Servicio de Hidrografia Naval, Armada Argentina.

SHN, 1986. Mar argentino, de Río de la Plata al Cabo de Hornos, fourth ed. Carta Náutica, vol. 50 Servicio de Hidrografia Naval, Armada Argentina.

SHN, 1992. Acceso al Río de la Plata, Carta Náutica H1, fifth ed. Servicio de Hidrografia Naval, Armada Argentina.

SHN, 1999a. Río de la Plata Exterior, Carta Náutica H113, second ed. Servicio de Hidrografia Naval, Armada Argentina.

SHN, 1999b. Río de la Plata Medio y Superior, Carta Náutica H116, fourth ed. Servicio de Hidrografia Naval, Armada Argentina.

SHN, 2018. Tablas de Marea. Publicación H-610. Servicio de Hidrografía Naval, Buenos Aires.

Simionato, C.G., Vera, C.S., Siegismund, F., 2005. Surface wind variability on seasonal and interannual scales over Río de la Plata Area. J. Coast Res. 214, 770–783. https://doi.org/10.2112/04-NIS.1.

Simionato, C.G., Meccia, V.L., Dragani, W.C., Guerrero, R.A., Nuñez, M.N., 2006a. The Río de la Plata estuary response to wind variability in synoptic to intra- seasonal scales: barotropic response. J. Geophys. Res. 111, C09031. https://doi.org/10.1029/2005JC003297.

Simionato, C.G., Meccia, V.L., Dragani, W.C., Nuñez, M.N., 2006b. On the use of the NCEP/NCAR surface winds for modeling barotropic circulation in the Río de la Plata Estuary. Estuar. Coast Shelf Sci. 70, 195–206. https://doi.org/10.1016/j.ecss.2006.05.047.

Simionato, C.G., Meccia, V.L., Guerrero, R.A., Dragani, W.C., Nuñez, M.N., 2007. The Río de la Plata estuary response to wind variability in synoptic to intra-seasonal scales: 2. Currents' vertical structure and its implications for the salt wedge structure. J. Geophys. Res. 112, C07005. https://doi.org/10.1029/2006JC003815.

Simmonds, I., Keay, K., 2000. Mean Southern Hemisphere extratropical cyclone behavior in the 40-year NCEP-NCAR reanalysis. J. Clim. 13, 873–885. https://doi.org/10.1175/1520-0442. (2000)013 < 0873:MSHECB > 2.0.CO;2.

SMN, 1992. Estadísticas Climatológicas 1981-1990. Serie B-N 37.

SMN, 2009. Estadisticas Climatologicas 1991–2000. Serie B-N 37.

Stopa, J.E., Ardhuin, F., Girard-Ardhuin, F., 2016. Wave climate in the arctic 1992-2014: seasonality and trends. Cryosphere 10, 1605–1629. https://doi.org/10.5194/tc-10-1605-2016.

Tokinaga, H., Xie, S.P., 2011. Wave- and Anemometer-based sea surface wind (WASWind) for climate change analysis. J. Clim. 24, 267–285. https://doi.org/10.1175/2010JCLI3789.1.

van de Koppel, J., van der Wal, D., Bakker, J.P., Herman, P.M.J., 2005. Self-organization and vegetation collapse in salt marsh ecosystems. Am. Nat. 165, E1–E12. https://doi.org/10.1086/426602.

Wang, X.L., Swail, V.R., 2001. 2001. Changes of extreme Wave Heights in northern Hemisphere Oceans and related atmospheric circulation regimes. J. Clim. 14, 2204–2221. https://doi.org/10.1175/1520-0442. 014 < 2204:COEWHI > 2.0.CO;2.

Wolters, M., Bakker, J.P., Bertness, M.D., Jefferies, R.L., Möller, I., 2005. Saltmarsh erosion and restoration in south-east England: squeezing the evidence requires realignment. J. Appl. Ecol. 42, 844–851. https://doi.org/10.1111/j.1365-2664.2005.01080.x.

Woolf, D.K., Challenor, P.G., Cotton, P.D., 2002. Variability and predictability of the North Atlantic wave climate. J. Geophys. Res. 107, 3145. https://doi.org/10.1029/2001JC001124.

Wray, R., Leatherman, S.P., Nicholls, R.J., 1995. Historic and future land loss for upland and marsh islands in the Chesapeake Bay, Maryland, U.S.A. J. Coast Res. 11, 1195–1203.

Young, I.R., Babanin, a. V., Zieger, S., 2011. Global Trends in Wind Speed and Waves Height. Science 332, 451–455. https://doi.org/10.1126/science.1197219.